NANO LETTERS

pubs.acs.org/NanoLett

Tunable Visible and Near-IR Emission from Sub-10 nm Etched Single-Crystal Si Nanopillars

Sameer S. Walavalkar,*,†,‡ Carrie E. Hofmann,†,‡ Andrew P. Homyk,†,‡ M. David Henry,†,‡ Harry A. Atwater,†,‡ and Axel Scherer†,‡

†Applied Physics Department, California Institute of Technology, 1200 East California Boulevard MC 200-36 Pasadena California 91125, United States, and ‡Kavli Nanoscience Institute, California Institute of Technology, 1200 East California Boulevard MC 107-81 Pasadena California 91125, United States

ABSTRACT Visible and near-IR photoluminescence (PL) is reported from sub-10 nm silicon nanopillars. Pillars were plasma etched from single crystal Si wafers and thinned by utilizing strain-induced, self-terminating oxidation of cylindrical structures. PL, lifetime, and transmission electron microscopy were performed to measure the dimensions and emission characteristics of the pillars. The peak PL energy was found to blue shift with narrowing pillar diameter in accordance with a quantum confinement effect. The blue shift was quantified using a tight binding method simulation that incorporated the strain induced by the thermal oxidation process. These pillars show promise as possible complementary metal oxide semiconductor compatible silicon devices in the form of light-emitting diode or laser structures.

KEYWORDS Silicon nanowires, plasma etching, photoluminescence, quantum effects, strain induced behavior

Silicon light emission is a rapidly growing area of inquiry. This field is uniquely important due to the dependence on silicon in the modern microelectronics industry. To economically create optical interconnects and circuit elements, the development of a silicon-compatible light emitter is critical, and the last two decades have shown marked advancement in the field of silicon light emission.[1]

Investigations into silicon light emission were instigated with the use of electrochemical reactions to etch large pores into single crystal silicon. The remaining structure behaved similar to one-dimensional (1D) quantum wires, resulting in visible and near-infrared photo- and electroluminescence.[1,2] Although the porous silicon consisted of structures small enough to create quantum confinement effects, there was some ambiguity over the actual source of the light emission. Some work indicated that the emission was due to Si−H complexes rather than quantum confinement[3] with light emission disappearing after the surface passivating hydrogen was heated off the sample.

To develop low-cost components, several groups utilized the technology developed for complementary metal oxide semiconductor (CMOS) processing to design nanoscale structures. Low-dimensional structures, such as nanopillars or nanocrystals patterned with "top-down" techniques are examples of these efforts.[2] Silicon nanocrystals have demonstrated both a wide emission bandwidth[4] and chemical stability. Unfortunately, the requirement for a wide band gap material as a cladding around the nanocrystal tends to prevent electrical excitation as wide band gap materials are typically insulators. Recent work,[5,6] however, has shown promise in utilizing floating gate devices to reliably excite nanocrystals. In such a device, holes and electrons are tunneled through a dielectric layer into the nanocrystals where they recombine.

A great deal of work has been done with grown[7−11] and etched[12−15] nanopillars. The vapor−liquid−solid (VLS) grown nanowires can be assembled as single crystals and present interesting electronic, optical, and structural properties. The standard catalyst used when growing silicon nanowires (SiNWs) in a chemical vapor deposition (CVD) reactor is gold; unfortunately, recent results have demonstrated[7] that such nanowires suffer from a deep-level trap resulting in a fast nonradiative decay, hindering PL. However, by using $TiSi_2$ as a catalyst[7,16] Guichard et al. have demonstrated size dependent PL in VLS grown nanowires. Depending on the crystal orientation of the substrate and the size of the catalyst particle VLS silicon tends to grow along the ⟨111⟩ or ⟨110⟩ crystal axes. On the basis of density functional theory (DFT) and tight binding method (TBM) simulations, wires grown along these axes have been predicted to not undergo a transition to a direct band gap as the wire diameter is decreased[17] unlike wires grown along the ⟨100⟩ direction.[18]

The alternative to bottom-up nanowire growth is top-down patterning via etching. The works cited above have shown that etched silicon pillars will photoluminescence, however previous work has not examined the relationship between the PL spectra and the size and surface conditions

* To whom correspondence should be addressed: E-mail: walavalk@caltech.edu.
Received for review: 06/17/2010
Published on Web: 10/04/2010

DOI: 10.1021/nl102140k | *Nano Lett.* **2010,** *10,* 4423–4428

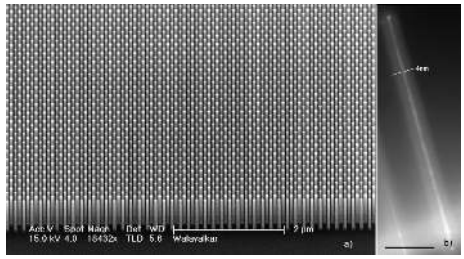

FIGURE 1. (a) An array of 50 nm pillars etched into single crystal silicon. (b) Reflection mode TEM image of 4 nm wide silicon core in an oxidized silicon nanopillar. Scale bar is 100 nm.

of the pillars. Previous attempts[14,12] have reported the spectral width of the PL emission to be greater than 1 eV. The wide spectral emission has been attributed to the distribution of pillar sizes in etched samples that masks the possible evolution of PL with respect to specific pillar diameter.

In this work, we fabricate top-down, etched, silicon nanopillars and further thin them via self-terminating oxidation to demonstrate photoluminescence as well as measure radiative lifetime with respect to reduction in pillar diameter. This behavior is obtained through the use of a novel aluminum oxide etch mask and etch technique as well as the utilization of the self-terminating properties of nanopillar oxidation to fabricate uniform, 1 μm tall pillars with diameters between 2 and 8 nm.

The fabrication of the nanowires follows Henry et al.[19] Pillars were defined by e-beam patterning an array of 30−50 nm disks in 75 nm of Micro-Chem PMMA 950 A2 on ⟨100⟩ silicon. A 25 nm layer of Al_2O_3 was deposited as a hard-mask via DC-magnetron sputtering of aluminum with a 5:1 Ar/O_2 process chemistry and patterned via lift-off. Aluminum oxide has been demonstrated as a resilient as well as chemically inert etch mask[19] providing a selectivity of greater than 60:1 for a fluorine etch chemistry. Etching was performed in an Oxford Plasmalab 100 ICP-RIE 380 machine running a "Pseudo Bosch" etch with simultaneous etching using SF_6 and passivation using C_4F_8, so-called mixed-mode etching. Sidewall profiles are controlled by adjusting the etch to passivation gas ratio. Figure 1a shows the uniformity in postetch profile of a pad of nanowires.

After etching, the pillars were oxidized in a dry ambient in the temperature range of 850−950 °C. Silicon core diameters were measured using reflection mode transmission electron microscopy (TEM) with the silicon pillars positioned perpendicular to the incoming electron beam. We were able to extract silicon core widths by utilizing the diffraction contrast between the crystalline Si and the amorphous SiO_2. A 4 nm wide silicon core imaged by this method is shown in Figure 1b. There has been extensive work[20−23] regarding the two-dimensional oxidation of cylindrical silicon structures. This work demonstrated that cylindrical silicon pillars exhibit a self-terminating core diameter and oxide thickness that is a function of the initial silicon

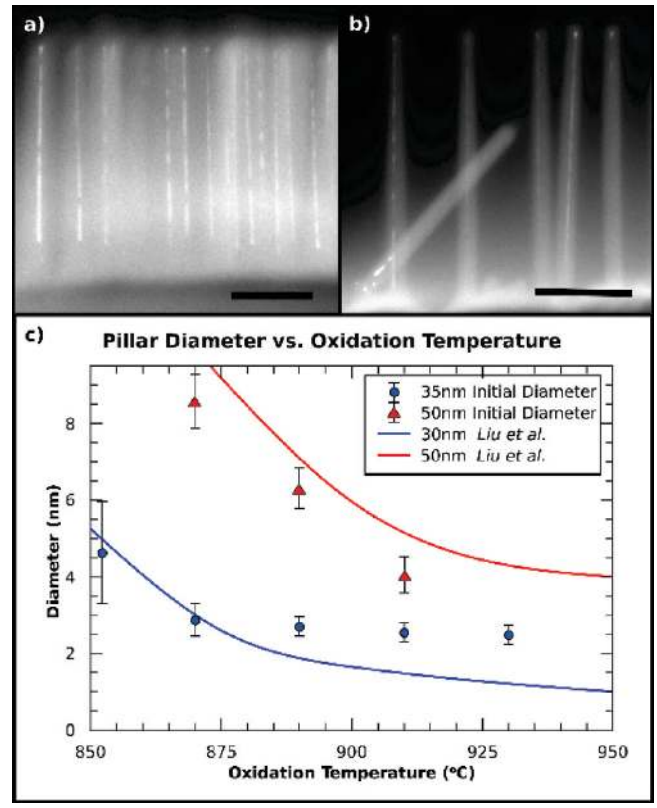

FIGURE 2. (a) TEM of a pad of 50 nm initial diameter pillars after oxidation at 890 °C. The single crystal silicon cores are bright compared to the amorphous silicon dioxide due to diffraction contrast. Scale bar is 200 nm. (b) TEM of the corner of a pad of 35 nm initial diameter pillars oxidized at 890 °C. (c) Tuning of pillar diameter based on oxidation temperature. The terminal pillar diameter is a function of both the initial diameter and the oxidation temperature. Included are the oxidation trends found in Liu et al. for 30 and 50 nm initial diameter pillars.

diameter and the temperature of the oxidation.[20] Several mechanisms have been proposed to explain this effect predicated on the idea that during oxidation at temperatures below 950 °C there is a lack of viscous flow of the grown oxide. The lattice mismatch between the silica and silicon creates a thin high-stress region at the $Si-SiO_2$ interface preventing diffusion of oxygen molecules or kinetically ruling out further oxidation. By oxidizing these pillars in the range of 850−950 °C for between 7 and 10 h we ensured that the final pillar diameter was equal to the saturation diameter reported in Liu et al.[20] Figure 2 shows the final pillar diameters as a function of initial diameter (35 or 50 nm) and oxidation temperature. Each data point represents the mean of 10−15 core diameters measured on a sample via reflection TEM and the error bars represent the standard deviation in the pillar size. Curves for oxidizing 30 and 50 nm pillars found in Liu et al.[20] are included in Figure 2 and we show good agreement with their predicted terminal core diameters. Variation between our data and their theory may stem from the fact that their model utilized experimental data to fit theory and extract parameters, such as oxygen diffusivity and reaction rate versus temperature, that would vary from

DOI: 10.1021/nl102140k | Nano Lett. 2010, 10, 4423–4428

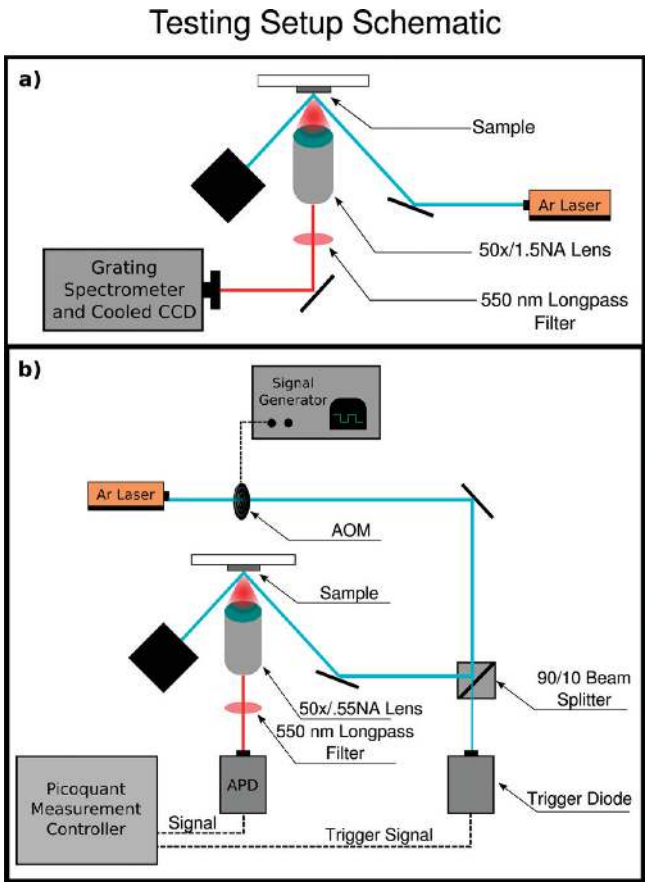

FIGURE 3. Schematic of the testing setup. (a) In the photoluminescence setup, laser light is used to pump the sample at a 45° angle and sent to a beam block while PL is collected through a microscope and sent through a 550 nm long pass filter to the cooled CCD camera. (b) For lifetime measurements, laser light is gated by an AOM with a period of 20 μs and 50% duty cycle and split with 90% of the light being sent to the sample and 10% to a trigger diode. PL collected from the sample is sent to an APD and the Picoquant controller uses the signal from the trigger diode to gate on and off the data collection from the APD to obtain lifetime measurements.

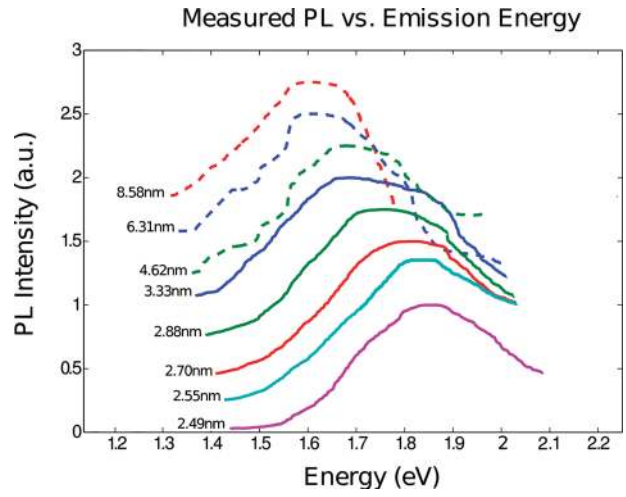

FIGURE 4. Normalized PL intensity from eight samples of various diameters. The variation in diameter was obtained by changing the oxidation temperature and the diameters reported are the average pillar size measured on a sample by reflection mode TEM. Dotted lines represent pillars with 50 nm initial diameters and continuous lines represent pillars with 35 nm initial diameters.

furnace to furnace and rely on the accuracy of calibration of the temperature controller governing the furnace. Figure 2a,b shows TEMs of 50 and 35 nm initial diameter pillars that have been oxidized at 890 °C.

Microphotoluminescence was performed on the samples by pumping with a free space Ar^+ ion laser at 488 nm. The sample was mounted in an inverted optical microscope, and the laser was shined onto the chip and reflected out into a beam block at a 45° angle to minimize the amount of laser light collected by the detection optics, Figure 3. The light was collected by a 50×/.55NA objective and passed through a 550 nm long-pass filter to further block the laser light. Finally, the light was passed to a grating spectrometer and then onto a cryogenically cooled Si CCD array.

Photoluminescence was observed between 600−800 nm (1.5−1.9 eV), as shown in Figure 4. The solid lines in Figure 4 indicate pillars with original diameters of 35 nm while the dashed lines are pillars with original diameters of 50 nm. The data shows a strong blue shift in peak emission wavelength corresponding to a decrease of the silicon core diameter. The peak wavelength versus core diameter is plotted in Figure 5a,b with the x error bars showing the standard deviation in pillar size while the y error bars show the full width half-maximum (fwhm) of the observed PL peak. From Figure 5a,b, the blue shift in peak PL energy correlates strongly with narrowing of the pillars, indicating that the emission energy is at least partially governed by a quantum confinement effect. We also note that our average fwhm is 240 meV with most widths at roughly 150 meV or less, roughly 30 to 50% narrower than previously reported results.[7,12,13] This narrow fwhm is indicative of a narrower size distribution of silicon pillar cores, an effect we believe is due in part to the better control over preoxidation pillar diameter via etching as well as allowing the pillars to reach a terminal diameter through a 7−10 h oxidation time.

Several methods were investigated to provide an explanation for the blue-shifted behavior of the peak emission, shown in Figure 5 as continuous lines. The simple effective mass theory that treats the confinement as an infinite quantum cylinder with the bulk silicon band gap as the unconfined ground state produced a trend that follows the $1/d^2$ expected of quantum confinement. As has been previously noted[24] this method underestimates the peak emission energy and a good description of the bands is required to model the emission of wires with diameters smaller than 10 nm. The second approach utilized a twenty band (ten valence, ten conduction) $sp^3s^*d^5$ tight binding approach[25,26] to calculate the bands between the Γ and X symmetry points. The results from this simulation are plotted in Figure 5. Although they provide a better fit to the data, this approach also tends to underestimate the emission energy. The final approach utilized the same tight binding simulation but incorporated the strain applied by the thermal oxidation

DOI: 10.1021/nl102140k | *Nano Lett.* **2010,** *10,* 4423–4428

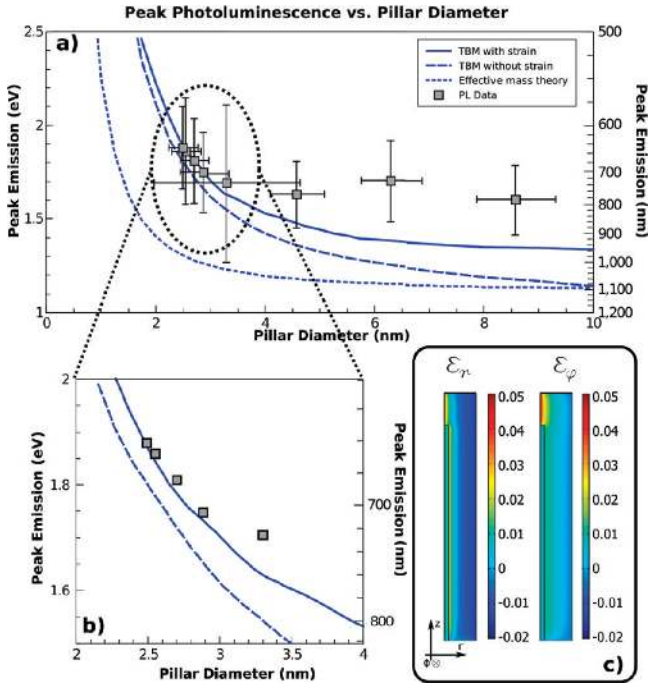

FIGURE 5. (a) Peak PL emssion as a function of terminal core diameter. Continuous lines represent three different theoretical explanations for the blue-shifted emission energy. Error bars in the *x*-direction represent standard deviation in pillar size and in the *y*-direction the fwhm of the measured PL. (b) Magnified view of peak emission for pillars between 2−4 nm. (c) Finite element strain model used to calculate the strain in the nanowires after oxidation. Shown is the strain in the radial and circumferential direction; the strain in the z-direction is negligible.

to deform the lattice. The strain was calculated using the parameters, such as core diameter and final oxide thickness, extracted from the TEM images and the methodology described elsewhere[20,21,23] as well as a finite element (FEM) simulation to calculate the strain induced by cooling the sample from oxidation to room temperature. The model that utilized in-plane tensile strain to deform the tight binding lattice provides a better fit to the peak emission data and indicates that the blue shift in emission wavelength is caused by a combination of both the strain as well as the quantum confinement.

Previous theoretical[17] and experimental[7,18] work has examined the role of strain in the energy and direct or indirect nature of the silicon band gap. While biaxial compressive strain tends to red shift the band energy, the biaxial tensile strain associated with oxidation[20,21] tends to blue shift the band gap[17,18] due to the bonding nature of the d orbital that contributes to the conduction band. From theoretical calculations based on Kao et al.[23] and Cui et al.[21] to compute the strain applied during oxidation as well as FEM analysis, we conclude that the pillars experience approximately 1.5% tensile strain in the radial and circumferential direction (Figure 5c) and negligible strain along the transverse direction. This is because the compressive strain associated with the thermal mismatch (between silicon and silicon dioxide) during the cool down to room temperature roughly cancels the tensile strain due to oxidation along the length of the pillar.

There has been extensive theoretical and experimental work that examines the role of oxidation and the silicon oxygen bond itself, in determining the band gap and peak emission energy in silicon nanocrystals. Two studies[27,28] have predicted that the presence of a silicon−oxygen double bond, as a result of the incomplete oxidation of silicon, creates a localized exciton state in nanocrystals with diameters of 2.5 nm or less. This state pins the band gap at 2.1 eV with the creation of a fast radiative trap state and effectively stops the band gap energy expansion due to quantum confinement. A variation of this effect was thought to be observed in these nanofabricated pillars when they were oxidized and allowed to return to room temperature in a nitrogen or oxygen ambient. A sharp peak was observed at 1.85−1.9 eV (650−670 nm) along with the wider peak associated with quantum confined PL. It was found that this sharp peak stayed at a fixed energy while the quantum confined PL would vary based on pillar size. Since the pillars were all larger than the threshold size of 2.5 nm, for the onset of the oxygen double bond pinning effect, and it was possible to see both sharp luminescence at 1.85 eV and broad band to band luminescence at longer wavelengths (Figure 6a), an alternative but similar mechanism was proposed. The presence of a nonbridging-oxygen hole center (NBOHC), typically found in a compressively strained silica matrix[29] and similar to the layers surrounding the silicon pillars under tensile strain, will serve to trap holes on isolated oxygen atoms and photoluminesce at 1.9 eV. Since the NBOHC is associated with localized states in the silica and not with the silicon itself, it is possible to simultaneously see PL from both NBOHC and band-to-band transitions in silicon. When the pillars were cooled to room temperature in forming gas (5% H_2, 95% N_2), instead of nitrogen, the peak at 1.9 eV disappeared. The suppression of the peak corresponds to a protonation and quenching of the NBOHC[29] via reactions with the rapidly diffusing molecular and atomic hydrogen.

Lifetime measurements were also taken of the measured samples. A 488 nm Ar^+ laser was passed through an acousto-optic modulator (AOM) that was gated with a square wave with a period of 20 μs and 50% duty cycle. The beam was sent to a 90/10 beam splitter where the majority of the light was sent to the sample and the rest of the light was sent to a trigger diode. The PL from the sample was collected by a 50×/.55NA lens and passed through a 550 nm long-pass filter onto an avalanche photodiode (APD). The signal from the APD was collected by the measurement controller (Picoquant Picoharp 300) when triggered by a signal from the trigger diode. Decay times were measured in the range of hundreds of nanoseconds and found to be decreasing with narrowing core diameter, Figure 6b. The inset in Figure 6b shows an example of the PL decay of a set of pillars with 2.88 nm average core diameter. The decreasing of PL

DOI: 10.1021/nl102140k | *Nano Lett.* **2010,** *10,* 4423–4428

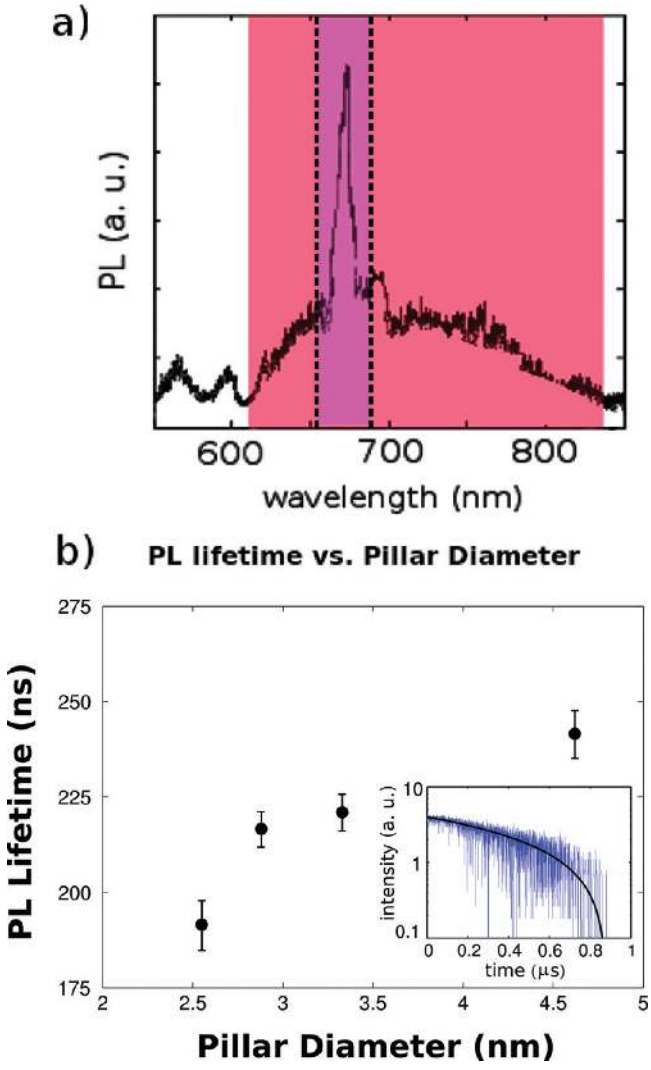

FIGURE 6. (a) Identification of PL peak associated with silica double bond defects. (b) Lifetime measurements for changing silicon core diameters. Error bars indicate uncertainty in the fit of the exponential decay time. Inset shows example of PL lifetime measurement with fitting curve in black.

lifetime with core diameter as well as the relatively short lifetimes (200 ns) can be attributed to several possible factors. Since the pillars prepared for this work were etched from Czochralski (CZ) grown silicon wafers the upper bound of the fast midgap nonradiative defect density is less than 10^7 cm^{-3} corresponding to a nonradiative lifetime of roughly 1 ms.[30,31] On the basis of diffraction contrast TEM images, the core material remains single crystal with any damage due to etching removed from the surface via oxidation. Furthermore the small volume occupied by the silicon cores would make it improbable to find such defects within the cores. This would indicate that PL lifetime in these etched pillars is governed by a radiative rather than nonradiative process. A possible mechanism for the transition to the radiative lifetime limited regime could be related to the magnitude of the splitting between the direct and indirect valleys of the conduction band. Theoretical calculations have

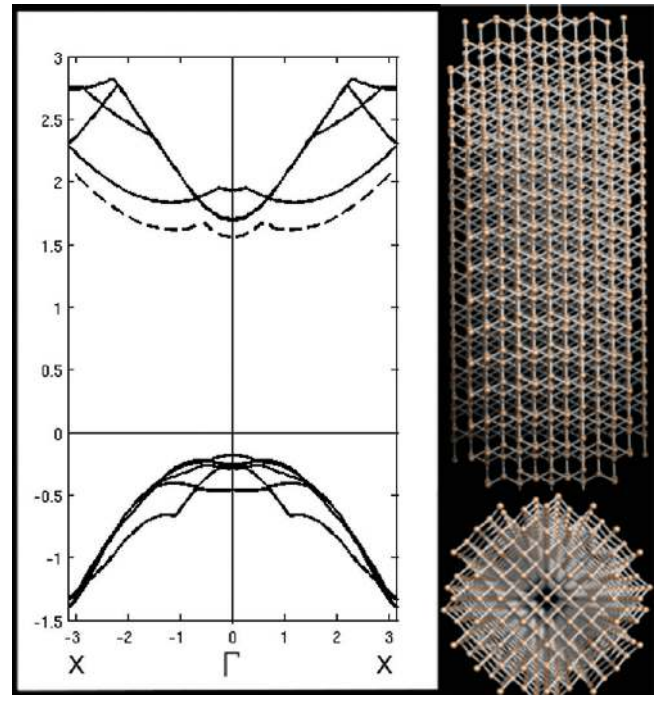

FIGURE 7. Band-structure (in eV) of a TBM simulation of a strained and unstrained 2.5 nm diameter silicon nanowire. The dotted line shows the relative conduction band edge for the unstrained wire while the two insets show the axial and transverse structure of the nanowire.

found the strain in nanowires to be important in increasing the splitting between the Γ conduction band valley and the bulk indirect X direction valley.[17,18] For pillars with diameters less than 10 nm experiencing tensile strain in the radial and circumferential direction, the splitting between these two minima is several times the room temperature thermal energy (depending on the wire diameter and the amount of strain), as seen in the solid lines of Figure 7. This large splitting allows the excited electrons to sit in the Γ valley, allowing for a faster, direct optical transition. For unstrained or compressively strained pillars (dotted line in Figure 7) the splitting between the two valleys is closer to the thermal energy forcing carriers to sit both in the Γ as well as the X valley, requiring a longer phonon-assisted recombination. Furthermore, by tuning the size of the pillars to be on order or smaller than the free-space electron wavelength, it is possible to increase the overlap between the hole and electron wave functions and therefore increase the recombination rate.[31] By examining the variation of radiative lifetime with temperature in future experiments it would be possible to determine the influence of the nonradiative decay as well. Guichard et al.[16] have shown that the bimolecular bound exciton Auger recombination coefficient of VLS grown nanowires scales with both temperature and the density of excitons. Since the pillars investigated in our report are both larger and smaller than the 4.9 nm ground state exciton radius in silicon,[32] it may be possible to see the onset of this effect as the size of the pillars crosses this

DOI: 10.1021/nl102140k | *Nano Lett.* **2010,** *10,* 4423–4428

threshold. Furthermore these pillars could serve as a platform to investigate the recombination dynamics of the "bulklike" excitons (excitons in structures larger than the exciton Bohr radius) as they transition into their 1D counterparts.

In conclusion, we have demonstrated room-temperature photoluminescence from silicon nanopillars etched from wafers of single crystal silicon. The uniformity in pillar diameter has allowed us to investigate the role of pillar diameter as well as oxidation strain in determining the peak emission energy. By varying the oxidation temperature we were able to show a blue shift in energy with decreasing core diameter that agrees with previous experimental work as well as tight-binding simulations. The fabrication process to create these pillars is fully CMOS-compatible and is a promising method to create integrated, visible and near-IR, on-chip silicon LED or laser devices.

Acknowledgment. S.W. would like to thank Imogen Pryce for her work on an early iteration of this project as well as Professor Tom Tombrello and Ryan Briggs for useful discussion. We would also like to gratefully acknowledge the Boeing Corporation under the CT-BA-GTA-1 grant and DARPA for generous support under the EPIC (HR0011-04-1-0054) and NACHOS (W911NF-07-1-0277) program. A.H. would like to thank the ARCS program for their support. M.D.H. would like to thank the John and Franny Hertz Foundation for their continued funding.

REFERENCES AND NOTES

(1) Fauchet, P. M. *IEEE J. Sel. Top. Quantum Electron.* **1998**, *4*, 1020–1028.
(2) *Light Emission from Nanoscale Silicon: The King of Microelectronics Advancing Toward Optoelectronic Integrated Circuits*, Rochester NY; Hirschman, K. D., Ed.; IEEE-Wiley e-Books Library: Online at: http://ieeexplore.ieee.org/xpls/abs_all.jsp?arnumber=616668, 1997, Vol. 177.
(3) Prokes, S. M.; Glembocki, O. J.; Bermudez, W. M.; Kaplan, R.; Friedersdorf, L. E.; Stevens, P. C. *Phys. Rev. B* **1992**, *45*, 13788–13791.
(4) Torre, J. D. L.; Souifi, A.; Poncet, A.; Busseret, C.; Lemiti, M.; Bremond, G.; Guillot, G.; Gonzales, O.; Garrido, B.; Morante, J. R.; Bonafos, C. *Physica E* **2003**, *16*, 326–330.
(5) Walters, R. J.; Bourianoff, G. I.; Atwater, H. A. *Nature* **2005**, *4*, 143–146.
(6) Beyer, V.; Schmidth, B.; Heining, K.-H.; Stegmann, K.-H. *Appl. Phys. Lett.* **2009**, *95*, 193501 1–3.
(7) Guichard, A. R.; Barsic, D. N.; Sharma, S.; Kamins, T. I.; Brongersma, M. L. *Nano Lett.* **2006**, *6*, 2140–2144.
(8) Demichel, O.; Oehler, F.; Calvo, V.; Noé, P.; Pauc, N.; Gentile, P.; Ferret, P.; Baron, T.; Magnea, N. *Physica E* **2009**, *41*, 963–965.
(9) Qi, J.; Belcher, A. M.; White, J. M. *Appl. Phys. Lett.* **2003**, *82*, 2616 1–3.
(10) Salhi, B.; Gelloz, B.; Koshida, N.; Patriarche, G.; Broukherroub, R. *Phys. Status Solidi* **2007**, *204*, 1302–1306.
(11) Noé, P.; Guignard, J.; Gentile, P.; Delamadeleine, E.; Calvo, V.; Ferret, P.; Dhalluin, F.; Baron, T. *J. Appl. Phys.* **2007**, *102*, No. 016103 1−3.
(12) Nassisopoulos, A. G.; Grigoropoulos, S.; Papadimitriou, D. *Appl. Phys. Lett.* **1996**, *69*, 2267–2269.
(13) Lewis, P. A.; Ahmed, H. *J. Vac. Sci. Technol., B* **1999**, *17*, 3239–3243.
(14) Tuovinen, C.; Malinin, A.; Ovchinnikov, V.; Toivola, T. *Phys. Scr.* **2002**, *101*, 125–128.
(15) Kolasinski, K. W.; Wellner, A.; Neuendorf, R.; Pedersen, C. X.; Palmer, R. E. *Photoluminescence from Silicon Nanostructures*; Central Laser Facility Annual Report 2000/2001; Rutherford Appleton Labs.: Didcot OX11 0QX. (Available online at: http://epubs.cclrc.ac.uk/work-details?w=28535).
(16) Guichard, A. R.; Kekatpure, R. D.; Brongersma, M. L.; Kamins, T. I. *Phys. Rev. B* **2008**, *78*, 235422.
(17) Peng, X.-H.; Alizadeh, A.; Bhate, N.; Varanasi, K. K.; Kumar, S. K.; Nayak, S. K. *J. Phys: Condens. Matter* **2007**, *19*, 266212 1–9.
(18) Audoit, G.; Mhuircheartaigh, E. N.; Lipson, S. M.; Morris, M. A.; Blau, W. J.; Holmes, J. D. *J. Mater. Chem.* **2005**, *15*, 4809–4815.
(19) Henry, M.; Walavalkar, S.; Homyk, A.; Scherer, A. *Nanotechnology* **2009**, *20*, 4.
(20) Liu, H. I.; Biegelsen, D. K.; Ponce, F. A.; Johnson, N. M.; Pease, R. F. W. *Appl. Phys. Lett.* **1993**, *64*, 1383–1385.
(21) Cui, H.; Wang, C. X.; Wang, G. W. *Nano Lett.* **2008**, *8*, 2731–2737.
(22) Buttner, C. C.; Zacharias, M. *Appl. Phys. Lett.* **2006**, *89*, 263106 1–3.
(23) Kao, D.-B.; McVittie, J. P.; Nix, W. D.; Saraswat, K. C. *IEEE Trans. Electron Devices* **1988**, *35*, 25–37.
(24) Delerue, C.; Allan, G.; Lanoo, M. *Phys. Rev. B* **1993**, *48*, 11024–11036.
(25) Wang, J.; Rahman, A.; Klimeck, G.; Lundstrom, M. *IEEE Int. Electron Devices Meet. Tech. Dig.* **2005**, *48*, 537–540.
(26) Paul, A.; Luisier, M.; Neophytou, N.; Kim, R.; Geng, J.; McLennan, M.; Lundstrom, M.; Klimeck, G. Band Structure Lab, 2006. http://nanohub.org/resources/1308 (accessed March 15, 2010).
(27) Luppi, M.; Ossicini, S. *Phys. Rev. B* **2005**, *71*, No. 035340.
(28) Wolkin, M. V.; Jorne, J.; Fauchet, P. M.; Allan, G.; Delerue, C. *Phys. Rev. Lett.* **1999**, *82*, 197–200.
(29) Griscom, D. *J. Ceram. Soc. Jpn.* **1991**, *99*, 923–942.
(30) Sadamitsu, S.; Umeno, S.; Koike, Y.; Hourai, M.; Sumita, S.; Shigematsu, T. *Jpn. J. Appl. Phys.* **1993**, *32*, 3675–3681.
(31) Singh, J. *Electronic and Optoelectronic Properties of Semiconductor Structures*, 1st ed.; Cambridge University Press: New York, 2003, Vol. 1.
(32) Beard, M. C.; Knutsen, K. P.; Yu, P.; Luther, J. M.; Song, Q.; Metzger, W. K.; Ellingson, R. J.; Nozik, A. J. *Nano Lett.* **2007**, *7*, 2506–2512.

DOI: 10.1021/nl102140k | *Nano Lett.* **2010,** *10,* 4423–4428